Reconfigurable Intelligent Surfaces Aided Wireless Communications with Electromagnetic Interference

Saber Hassouna , Muhammad Ali Jamshed , Masood Ur-Rehman , Muhammad Ali Imran , and Qammer H. Abbasi

James Watt School of Engineering, University of Glasgow, Glasgow, U.K
Email:s.hassouna.1@research.gla.ac.uk
{muhammadali.jamshed,masood.urrehman,muhammad.imran,qammer.abbasi}@glasgow.ac.uk

***Abstract*—Controlling the electromagnetic signals' features of scattering, reflection, and refraction is possible using reconfigurable intelligent surfaces (RIS). In this study, we examined the data rate performance utilizing a codebook technique to produce a set of pre-designed phase shift configurations for the RIS elements. This arrangement has previously been investigated without taking into account electromagnetic interference (EMI), which consists of the inescapable incoming waves from outside sources. We analyzed the system model considering the EMI for single-user SISO wideband communication system. We developed the power method to get a high-quality optimized configuration for the RIS besides using the old water pouring algorithm to fairly allocate the power for all orthogonal frequency division multiplexing (OFDM) subcarriers. Communication performance is significantly impacted by electromagnetic interference, particularly as the RIS becomes bigger.**

***Index Terms*—Reconfigurable Intelligent Surfaces (RIS), Orthogonal Frequency Division Multiplexing (OFDM), Electromagnetic Interference (EMI) and Data Rate.**

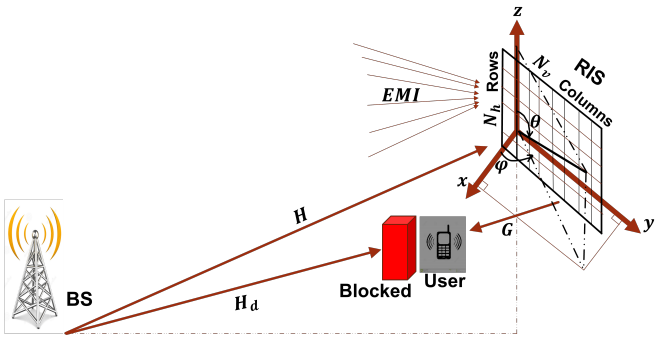

Fig. 1. System Setup.

I. Introduction

In the field of wireless communication research, reconfigurable intelligent surfaces (RISs) have lately come to light as a cutting-edge method. Intelligent surfaces with electromagnetic material bases are known as RISs. RISs are Microelectronic circuits with wireless communication capabilities are used to regulate the materials, enabling them to handle wireless propagation circumstances in a way that was not before possible [1], [2], [3]. The RISs are composed of a large number of small, inexpensive passive components that have the ability to modify wireless signals in a manner that is not possible with conventional materials and surfaces.

RIS-assisted communication may allow signal focusing at the receiver thanks to the constructive superposition of the line of sight (LOS) route between the transmitter and receiver as well as reflections from all of the RIS's metasurface components that create a beam in a specific direction [4]. The channel between the transmitter and receiver may be improved by using wireless repeaters, relays, and reflect array antennas, as examples of earlier technology [5]. Some of the properties that make RISs unique include the fact that they can be programmed and do not need power amplifiers, sophisticated processing, or encoding and decoding algorithms [6]. Recently, many efforts have been made to enhance various performance metrics in RIS-assisted communication systems [7].

A significant amount of past work on RIS has focused on a single-input single-output (SISO), multiple-input single-output (MISO) and multiple-input multiple output (MIMO) setup [8], [9], [10]. However, these prior works did not consider the EMI in their works [11].

Against the above and in this paper, we investigated the data rate in relation to phase tuning and power allocation at the presence of EMI. Power Allocation for the entire subcarriers can be resolved by a solution called Water-Pouring. For configuring the RIS, we used the pre-designed phase shift configurations generated by the beamforming codebook approach to help us configuring the RIS surface. For Large surfaces $N = 4096$ elements, The DFT matrix's column [12] can be used to represent the reflection coefficiens. We select the best signal to noise ratio (SNR) configuration from the built codebook, to be used in the iterative algorithm to get the optimal RIS configuration. We noticed the effect of EMI on the data rate and the remarkable difference in the data rate between the case when EMI is existed and the case without EMI consequently, the EMI should be considered in the future research. An overview of the remainder of the paper is provided below. The system model is introduced in Section II. The EMI and channel model is the focus of Section III, while section IV present the codebook approach and the iterative algorithm. We show the simulation results in section

V. Finally, in part VI, there is a conclusion.

II. System Model

We go through how to communicate with only single antenna base station (BS) to single user using an RIS with N reconfigurable controllable elements which is organized into a uniform planar array with $N_H = 64$ elements per horizontal row and $N_V = 64$ elements per vertical column as per Fig. 1. We presume that OFDM is being used for the transmission. The system's entire bandwidth is evenly split into $\mathcal{K}$ orthogonal subcarriers, like typical OFDM-based systems. The total power for all subcarriers is $\mathcal{P} = \frac{1}{\mathcal{K}} \sum_{\kappa=0}^{\mathcal{K}-1} p_k$ where $p_0, \ldots, p_{\mathcal{K}-1}$ is the power given to subcarrier k. Let the direct channel $H_d = [H_d[0], \ldots\ldots, H_d[\mathcal{M}-1]]^T \in \mathbb{C}^{\mathcal{M}\times 1}$ represents all the uncontrollable channel components. Additionally, there is a $\mathcal{M}$-tap baseband equivalent multipath channel for the BS-RIS-user link via which the RIS reflects the signal that the BS transmits before it reaches the user consequently, let $H = [h_0, \ldots, h_{\mathcal{M}-1}] \in \mathbb{C}^{N\times\mathcal{M}}$ is the BS-RIS channel where $h_l \in \mathbb{C}^{N\times 1}$ corresponds to the l-th tap, $0 \le l \le \mathcal{M}-1$ while $G = [g_0, \ldots, g_{\mathcal{M}-1}] \in \mathbb{C}^{N\times\mathcal{M}}$ is the RIS-User channel where $g_l^H \in \mathbb{C}^{1\times N}$ corresponds to the l-th tap, $0 \le l \le \mathcal{M}-1$. When the signal is received at the RIS, each element re-scatters it with a different reflection coefficient so, $w_\theta = \operatorname{diag}\left(e^{j\theta_1}, e^{j\theta_2}, \ldots, e^{j\theta_N}\right)$ is the diagonal matrix that holds the RIS's reflection coefficients. For the sake of clarity, let us denote $V = [v_0, \ldots, v_{\mathcal{M}-1}] \in \mathbb{C}^{N\times\mathcal{M}}$ where $v_l^H = g_l^H \operatorname{diag}(h_l) \in \mathbb{C}^{1\times N}$. Then we have $v_l^H w_\theta = g_l^H w_\theta h_l$ that characterizes the BS-RIS-User composite channel at the l-th tap. The signal at the receiver $z_k \in \mathbb{C}$ at the k-th subcarrier $k = 0, \ldots, \mathcal{K}-1$ using the discrete Fourier transform (DFT) at the RIS is given [11]:

$$z_k = H_k x_k + e_{EMI} \tag{1}$$

where x_k is the transmitted signal and $e_{EMI} \sim \mathcal{N}_{\mathbb{C}}\left(0, A\sigma^2 R\right) \in \mathbb{C}$ is the EMI generated by the approaching uncontrollable signals [11]. We will discuss and define the EMI parameters in section III. The received signal $r_k \in \mathbb{C}$ is given as per Fig. 1:

$$r_k = z_k w_\theta G_k^H + H_d x_k + e_k \tag{2}$$

where $e_k \sim \mathcal{N}_{\mathbb{C}}\left(0, \sigma_e^2\right)$ is the receiver noise affecting the received signal apart from reflected EMI by the RIS. By substituting (1) in (2).

$$r_k = \left(G_k^H w_\theta H_k + H_d\right) x_k + w_\theta G_k^H e_{EMI} + e_k \tag{3}$$

Let us denote $h_\theta = \left(G_k^H w_\theta H_k + H_d\right)$ and $\mathcal{G} = w_\theta G_k^H$. We can represent (3) in a vector form as follows:

$$\begin{bmatrix} \bar{r}[0] \\ \vdots \\ \bar{r}[\mathcal{K}-1] \end{bmatrix} = \begin{bmatrix} \bar{h}_\theta[0] \\ \vdots \\ \bar{h}_\theta[\mathcal{K}-1] \end{bmatrix} \odot \begin{bmatrix} \bar{x}[0] \\ \vdots \\ \bar{x}[\mathcal{K}-1] \end{bmatrix} + \begin{bmatrix} \overline{\mathcal{G}}\bar{e}_{EMI}[0] \\ \vdots \\ \overline{\mathcal{G}}\bar{e}_{EMI}[\mathcal{K}-1] \end{bmatrix} + \begin{bmatrix} \bar{e}[0] \\ \vdots \\ \bar{e}[\mathcal{K}-1] \end{bmatrix} \tag{4}$$

where $\odot$ denotes the Hadamard product. The output of the OFDM block can be described in a short form as follows:

$$\bar{r} = \bar{h}_\theta \odot \bar{x} + \bar{\mathcal{G}}\bar{e}_{EMI} + \bar{e} \tag{5}$$

We notice that the channel frequency response of $\bar{h}_\theta$:

$$\bar{h}_\theta = \mathcal{F}\begin{bmatrix} H_d[0] + v_0^H w_\theta \\ \vdots \\ H_d[\mathcal{M}-1] + v_{\mathcal{M}-1}^H w_\theta \end{bmatrix} = \mathcal{F}\left(H_d + V^H w_\theta\right) \tag{6}$$

where $\mathcal{F}$ is a $\mathcal{K}\times\mathcal{M}$ DFT Matrix. The channel frequency response at each k-th subcarrier is given as:

$$h_{\theta_k} = f_k^H H_d + f_k^H V^H w_\theta, \quad k = 0, \ldots, \mathcal{K}-1 \tag{7}$$

where f_k^H denotes the k-th row of the DFT matrix $\mathcal{F}$. Consequently, we can represent the sum data rate over the $\mathcal{K}$ subcarriers for equal power distribution, certain phase configuration w_θ and known channel state information at the receiver:

$$\mathcal{R} = \frac{\mathcal{B}}{\mathcal{K}+\mathcal{M}-1} \sum_{k=0}^{\mathcal{K}-1} \log_2\left(1 + \frac{\mathcal{P}\left|f_k^H H_d + f_k^H V^H w_\theta\right|^2}{A\sigma^2 \mathcal{G}^H R \mathcal{G} + \sigma_e^2}\right) \frac{\text{bit}}{s} \tag{8}$$

In (8), we did consider the effect of the e_{EMI} and $\mathcal{B}$ is the total bandwidth.

III. EMI and Channel Model

1) EMI Model: The EMI e_{EMI} is generated by a superimposed cline of approaching plane signals from outside sources. It is modeled as in corollary1 [11] and distributed as $e_{EMI} \sim \mathcal{N}_{\mathbb{C}}\left(0, A\sigma^2 R\right)$ where A is the RIS element area, σ^2 is the interference power and the (n,m)-th unit of R is given by:

$$[\mathrm{R}]_{n,m} = \iint_{-\pi/2}^{\pi/2} e^{j\mathcal{W}(\varphi,\theta)^{\mathrm{T}}(\mathbf{u}_n - \mathbf{u}_m)} \alpha(\varphi,\theta) d\varphi d\theta \tag{9}$$

where $\mathcal{W}(\varphi,\theta) = \frac{2\pi}{\lambda}[\cos(\theta)\cos(\varphi), \cos(\theta)\sin(\varphi), \sin(\theta)]^{\mathrm{T}}$ is the wave number that describes the phase changes of the plane waves, φ is the azimuth angle and θ is the elevation angle. $\alpha(\varphi,\theta)$ is the power angular density with $\iint_{-\pi/2}^{\pi/2} \alpha(\varphi,\theta) d\varphi d\theta = 1$ and $\boldsymbol{u}_n = [0, i(n)d_v, j(n)d_h]^{\mathrm{T}}$ is the location of the n-th element with $n \in [1, N]$. d_v and d_h are the vertical and horizontal elements spacing where, $d_v^2 = d_h^2 = A$. While $i(n)$ and $j(n)$ are the horizontal and vertical indices of element n. Under circumstances of isotropic distribution (i.e., uniform distribution from all angles), (9) can be reduced to Prop1 [13]:

$$[R]_{n,m} = \operatorname{sinc}\left(\frac{2\left\|\mathbf{u}_n - \mathbf{u}_m\right\|}{\lambda}\right) \tag{10}$$

where $\|\cdot\|$ is the Euclidean norm.

A. Channel Model and propagation environment

We assume that the system has a perfect channel model. Specifically, the following channel is used [3]:

$$H_d = \sum_{l=1}^{L_d} \sqrt{B_{d,l}} e^{-j2\pi f_c \tau_{d,l}} \begin{bmatrix} \operatorname{sinc}\left(0 + \mathcal{B}\left(\gamma - \tau_{d,l}\right)\right) \\ \vdots \\ \operatorname{sinc}\left(\mathcal{M} - 1 + \mathcal{B}\left(\gamma - \tau_{d,l}\right)\right) \end{bmatrix} \tag{11}$$

where $B_{d,l} \geq 0$ is the pathloss of the l-th path, L_d is the multipath number, $\tau_{d,l}$ is the propagation delay and γ is the sampling delay over the shortest path. Similarly, the controllable path is given by:

$$V = \sum_{l=1}^{L_a} \sum_{\ell}^{L_b} \sqrt{B_{a,l} B_{b,\ell}} e^{-j2\pi f_c (\tau_{a,l} + \tau_{b,\ell})} \left(a\left(\varphi_{a,l}, \theta_{a,l}\right) \odot a\left(\varphi_{b,\ell}, \theta_{b,\ell}\right)\right) \begin{bmatrix} \operatorname{sinc}\left(0 + \mathcal{B}\left(\gamma - \tau_{d,l} - \tau_{b,\ell}\right)\right) \\ \vdots \\ \operatorname{sinc}\left(\mathcal{M} - 1 + \mathcal{B}\left(\gamma - \tau_{d,l} - \tau_{b,\ell}\right)\right) \end{bmatrix}^T \tag{12}$$

The propagation paths L_a and L_b from the BS to the RIS and from the RIS to the user, respectively. $B_{a,l} \geq 0$, and $B_{b,\ell} \geq 0$, are the pathlosses from the BS to the RIS and from the RIS to the user respectively. $\tau_{a,l}$ and $\tau_{b,\ell}$ are the propagation delays to and from the RIS. All the parameters are considered by using the 3GPP channel model [14], [15]. The LOS is considered for the indirect channel BS-RIS-User however, the channel between the BS and the user experiences non-(LOS). The RIS under consideration has $N = 4096$ elements and is organized as a uniform planar array with $N_h = 64$ elements per horizontal row and $N_v = 64$ elements per vertical column. The array is located in the yz plane according to the system setup shown in Fig. 1.

IV. Beamforming Codebook and Iterative Algorithim

Contrary to the narrowband case, when there is just one channel (one subcarrier), RIS optimization in the wideband scenario is more challenging because there are $\mathcal{K}$ parallel subcarriers. The most optimal vector w_θ is necessary for the optimization of (8) with regard to RIS configuration. For a one-bit RIS design, each RIS element may only accept two possible phase shifts, either $\pi/2$ or $-\pi/2$. We inspired the generation of such phase matrices from the beamforming codebook of the RIS [12], [16], [17].

A. Beamforming Codebook

If there is any realistic chance of finding a configuration that is near to the best one out of the 2^N possible RIS configurations, then choosing one of them would have to be extraordinarily difficult. Existing research relies on high-precision configurations, in which a RIS with N reflecting elements may switch between N mutually orthogonal configurations. For a particular angle of incidence and reflection, the 2D-DFT codebook's design of the RIS phase shifts remains valid [12]. Consequently, each column of the codebook beamform $W_\theta = \mathcal{F}\left(N_v\right) \otimes \mathcal{F}\left(N_h\right) \in \mathbb{C}^{N \times N}$ can be a possible reflection configuration for an incident signal in a specific direction of propagation. Let $\otimes$ denotes the Kronecker product. The DFT matrices for the columns $\mathcal{F}\left(N_v\right)$ and $\mathcal{F}\left(N_h\right)$ can be denoted as:

$$\mathcal{F}\left(N_v\right) = \begin{bmatrix} 1 & 1 & 1 & \cdots & 1 \\ 1 & f_{N_v} & f_{N_v}^2 & \cdots & f_{N_v}^{N_v-1} \\ \vdots & \vdots & \vdots & \vdots & \vdots \\ 1 & f_{N_v}^{N_v-1} & f_{N_v}^{2(N_v-1)} & \cdots & f_{N_v}^{(N_v-1)(N_v-1)} \end{bmatrix} \tag{13}$$

where $f_{N_v} = e^{-j2\pi/N_v} = \cos\left(2\pi/N_v\right) - \sin\left(2\pi/N_v\right)$. The phase shifts generated by the codebook must be quantized to meet the design of the RIS. As a result, the reflection coefficient w_θ for element i can be either $e^{j\pi/2}$ if $\arg\left(\left[w_\theta\right]_i\right) \in [-\pi, 0)$ or $e^{-j\pi/2}$ if $\arg\left(\left[w_\theta\right]_i\right) \in [0, \pi)$ [12]. We searched in the codebook W_θ for the best configuration that maximize the SNR:

$$SNR = \frac{\mathcal{P}\left|\bar{h}_\theta\right|^2}{A\sigma^2 \mathcal{G}^H R \mathcal{G} + \sigma_e^2} = \frac{\mathcal{P}\left|H_d + V^H w_\theta\right|^2}{A\sigma^2 \mathcal{G}^H R \mathcal{G} + \sigma_e^2} \tag{14}$$

We deliberately mention the signal to noise ratio because we consider the interference as a noise. Let us denote the best phase configuration that can be generated from the codebook is $w_{\theta_{\text{CodeBook}}} \in W_\theta$ which will be utilized later in the power iterative algorithm.

B. RIS Optimization with the knoweledge of EMI

1) Iterative Power Algorithim: In this paper, we look at the issue of maximizing the sum data rate at the user by finding the optimal transmit power $\mathcal{P}$ to be distributed across all subcarriers based on the power limitation for each subcarrier and the optimal phase matrix w_θ for all RIS elements. However, It is worthwhile to optimize if configuring the RIS relies on the EMI and the awareness of the spatial correlation matrix R would result in a higher data rate. Let us neglect the direct channel and rewrite (14) as follows:

$$SNR = \frac{\mathcal{P}}{\sigma_e^2} \frac{w_\theta^H \mathcal{A} w_\theta}{w_\theta^H Q w_\theta + 1} \tag{15}$$

where $\mathcal{A} = VV^H$ and $Q = \frac{A}{\sigma_e^2}\sigma^2 \mathcal{G}^H R \mathcal{G}$. Consequently, we can represent (15) as:

$$SNR = \frac{\mathcal{P}}{\sigma_e^2} \frac{w_\theta^H \mathcal{A} w_\theta}{w_\theta^H \mathcal{C} w_\theta} \tag{16}$$

where $\mathcal{C} = Q + I_N$. So, it is necessary to address the following problem in order to maximise the SNR in (16):

$$\begin{aligned} \max_{\mathcal{P}, w_\theta, \bar{w}_\theta} \quad & \left(\bar{w}_\theta^H \mathcal{D} \bar{w}_\theta\right) \\ \text{s.t} \quad & \left|\left[w_\theta\right]_i\right| = 1, \qquad \forall_i \in N \\ & \bar{w}_\theta = \mathcal{C}^{1/2} w_\theta \\ & \tfrac{1}{\mathcal{K}} \textstyle\sum_{k=0}^{\mathcal{K}-1} p_k \leq \mathcal{P}, \\ & p_k \geq 0, \qquad \forall_k \in \mathcal{K} \end{aligned} \tag{17}$$

where $\mathcal{D} = \left(\mathcal{C}^{-1/2}\right)^H \mathcal{A} \mathcal{C}^{-1/2}$. The optimization problem is non-convex over the unit modular constraint on all RIS

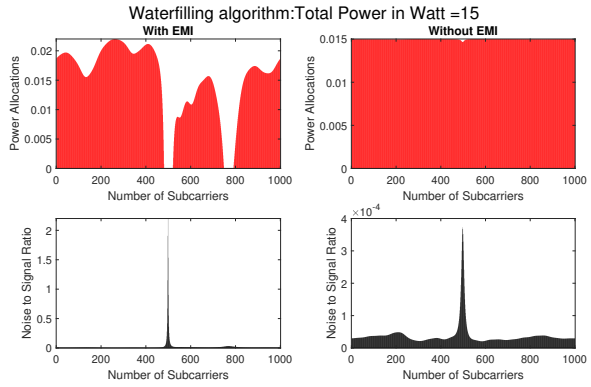

Fig. 2. Power allocation for subcarriers in two cases: with and without EMI

elements and the vector w_θ does not vary with the subcarrier index k. This constraint ensures that each RIS element's reflection has no pathloss. Furthermore, unlike relays, RIS components do not amplify or decode then convey a received signal, necessitating the use of unit magnitude RIS elements. The iterative power method can be used to overcome the non-convexity by beginning the computation $\bar{w}_{\theta_{i+1}} = \frac{\mathcal{D}\bar{w}_{\theta_i}}{\|\mathcal{D}\bar{w}_{\theta_i}\|}$ from initial solution $\bar{w}_{\theta_0}$. The initial solution can be selected to be the best configuration from the codebook $\bar{w}_{\theta_0} = w_{\theta_{\text{CodeBook}}}$ and then compute $\mathcal{D}\bar{w}_{\theta_i}$ and after that quantize phases of all candidates $\arg\left([w_\theta]_i\right)$ where $i = 1, \ldots, N$ to be either $\left\{e^{j\pi/2}\right.$ or $\left.e^{-j\pi/2}\right\}$ if $\arg\left([w_\theta]_i\right) \in [-\pi, 0)$ and $\arg\left([w_\theta]_i\right) \in [0, \pi)$ respectively. Finally iterate until convergence.

2) Water-Pouring Algorithm : Moreover, the power $\mathcal{P}$ should be optimized all over the subcarriers. The power distribution for all subcarriers $p_0, \ldots, p_{\mathcal{K}-1}$ are satisfying $\mathcal{P} = \frac{1}{\mathcal{K}} \sum_{k=0}^{\mathcal{K}-1} p_k$ where $p_k = E\left\{|\bar{x}[k]|^2\right\}$ is the power related to subcarrier k. Taking into account the EMI, The power allocation for the subcarriers can be optimized by the water-pouring algorithm [3].

$$p_k = \max\left(\mu - \frac{A\sigma^2 \mathcal{G}^H R \mathcal{G} + \sigma_e^2}{|f_v^H H_d + f_v^H V^T w_\theta|^2}, 0\right) \tag{18}$$

Where the parameter $\mu \geq 0$ is chosen to fulfil $\frac{1}{\mathcal{K}} \sum_{k=0}^{\mathcal{K}-1} p_k = \mathcal{P}$. Consequently, the power allocated for k-th subcarrier p_k is dependent on the water level parameter μ.

The water-pouring algorithm is used to allocate the transmitted power fairly to all subcarriers where the weak channel gain is allocated less power while the strong channel gain is allocated more power however, the total allocated power should not exceed the total power (15 Watt) as per Fig. 2. In Fig. 2, we show comparison for the power allocation between the cases with and without EMI to demonstrate how the algorithm allocate the power to each subcarrier taking into consideration the channel gain status.

V. Simulation Results

In this part, we provide simulation results to assess the performance of the iterative algorithm for optimizing the achievable data rate of RIS-assisted SISO-OFDM system. Table I shows the system parameters used in the Monte Carlo simulations.

TABLE I
Simulation Parameters

System Parameter	Simulation value
Carrier frequency f_c	4e9 Hz
Speed of light	3e8 m/s
Wavelength λ	0.075 m
Number of elements N	4096
BS Location in meter	$\begin{bmatrix} 40 & -150 & 0 \end{bmatrix}^T$
User Location in meter	$\begin{bmatrix} 20 & 0 & 0 \end{bmatrix}^T$
Pathloss Model non-LOS	$34.53 + 38\log_{10}(d)$
Pathloss Model LOS	$30.18 + 26\log_{10}(d)$
L_a,L_b and L_d	100, 51 and 100 respectively
Number of channel taps $\mathcal{M}$	23
Number of subcarriers $\mathcal{K}$	1000
Transmit Power $\mathcal{P}$	15 Watt
Bandwidth $\mathcal{B}$	15e6 Hz

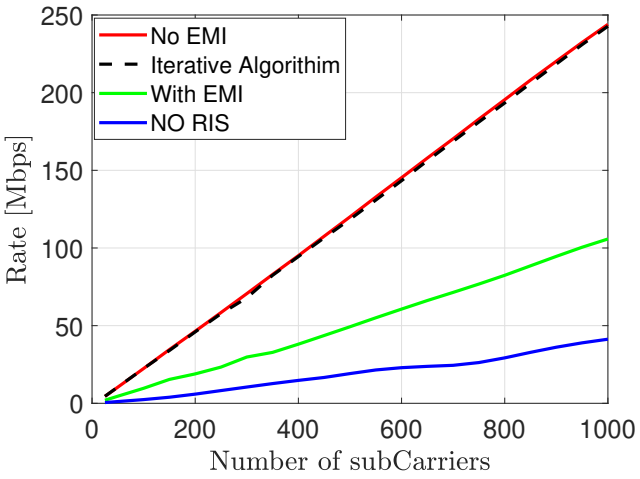

Fig. 3. Data Rate against number of Subcarriers with and without EMI

In Fig. 3, we considered the case when there is no EMI is the reference to be compared with the cases with EMI and uniform surface (NO RIS). There is a remarkable difference between the cases with and without EMI so the iterative algorithm enhanced the rate to be very close to the case without EMI. Consequently, the RIS must be aware of EMI in order to get higher data rate for the user.

VI. Conclusion

In this paper we proved that the effect of EMI is inevitable in RIS aided wireless communication. RIS data rates are investigated under different scenarios and finally compared with the case of NO EMI. The analysis revealed that, particularly when the number of passive elements N increases significantly, EMI may have a severe effect on the data rate. The codebook

approach was implemented to generate varieties of phase configurations for the RIS surface in which we searched for the best configuration to be used in the optimization process. We initialize the iterative algorithm with the best configuration generated from the codebook. The information rate resulted from the iterative algorithm is very close to the reference case without EMI, so the RIS must be aware of the EMI and the EMI should be considered in the analysis of RIS aided communication. Since RIS technology and 6G research are linked, it is imperative to find improved communication models that take advantage of electromagnetic features and are compatible with practical applications.

REFERENCES

[1] C. Liaskos, S. Nie, A. Tsioliaridou, A. Pitsillides, S. Ioannidis, and I. Akyildiz, "A new wireless communication paradigm through software-controlled metasurfaces," *IEEE Communications Magazine*, vol. 56, no. 9, pp. 162–169, 2018.

[2] Q. Wu and R. Zhang, "Intelligent reflecting surface enhanced wireless network via joint active and passive beamforming," *IEEE Transactions on Wireless Communications*, vol. 18, no. 11, pp. 5394–5409, 2019.

[3] E. Björnson, H. Wymeersch, B. Matthiesen, P. Popovski, L. Sanguinetti, and E. de Carvalho, "Reconfigurable intelligent surfaces: A signal processing perspective with wireless applications," *IEEE Signal Processing Magazine*, vol. 39, no. 2, pp. 135–158, 2022.

[4] E. Björnson, Ö. Özdogan, and E. G. Larsson, "Intelligent reflecting surface versus decode-and-forward: How large surfaces are needed to beat relaying?" *IEEE Wireless Communications Letters*, vol. 9, no. 2, pp. 244–248, 2019.

[5] ——, "Reconfigurable intelligent surfaces: Three myths and two critical questions," *IEEE Communications Magazine*, vol. 58, no. 12, pp. 90–96, 2020.

[6] M. Di Renzo, K. Ntontin, J. Song, F. H. Danufane, X. Qian, F. Lazarakis, J. De Rosny, D.-T. Phan-Huy, O. Simeone, R. Zhang *et al.*, "Reconfigurable intelligent surfaces vs. relaying: Differences, similarities, and performance comparison," *IEEE Open Journal of the Communications Society*, vol. 1, pp. 798–807, 2020.

[7] Z. S. WU QQ, B. ZHENG *et al.*, "Intelligent reflecting surface-aided wireless communications: a tutorial [j]," *IEEE transactions on communications*, vol. 69, no. 5, pp. 3313–3351, 2021.

[8] Q. Wu and R. Zhang, "Intelligent reflecting surface enhanced wireless network via joint active and passive beamforming," *IEEE Transactions on Wireless Communications*, vol. 18, no. 11, pp. 5394–5409, 2019.

[9] X. Yu, D. Xu, and R. Schober, "Miso wireless communication systems via intelligent reflecting surfaces," in *2019 IEEE/CIC International Conference on Communications in China (ICCC)*. IEEE, 2019, pp. 735–740.

[10] Y. Yang, B. Zheng, S. Zhang, and R. Zhang, "Intelligent reflecting surface meets ofdm: Protocol design and rate maximization," *IEEE Transactions on Communications*, vol. 68, no. 7, pp. 4522–4535, 2020.

[11] A. de Jesus Torres, L. Sanguinetti, and E. Björnson, "Electromagnetic interference in ris-aided communications," *IEEE Wireless Communications Letters*, vol. 11, no. 4, pp. 668–672, 2021.

[12] X. Pei, H. Yin, L. Tan, L. Cao, Z. Li, K. Wang, K. Zhang, and E. Björnson, "Ris-aided wireless communications: Prototyping, adaptive beamforming, and indoor/outdoor field trials," *IEEE Transactions on Communications*, vol. 69, no. 12, pp. 8627–8640, 2021.

[13] E. Björnson and L. Sanguinetti, "Rayleigh fading modeling and channel hardening for reconfigurable intelligent surfaces," *IEEE Wireless Communications Letters*, vol. 10, no. 4, pp. 830–834, 2020.

[14] Spatial channel model for multiple input multiple output (mimo) simulations (release 16). [Online]. Available: https://portal.3gpp.org/desktopmodules/Specifications/SpecificationDetails.aspx?specificationId=1382

[15] E. Björnson, "Optimizing a binary intelligent reflecting surface for ofdm communications under mutual coupling," in *WSA 2021; 25th International ITG Workshop on Smart Antennas*. VDE, 2021, pp. 1–6.

[16] J. Mao, Z. Gao, Y. Wu, and M.-S. Alouini, "Over-sampling codebook-based hybrid minimum sum-mean-square-error precoding for millimeter-wave 3d-mimo," *IEEE Wireless Communications Letters*, vol. 7, no. 6, pp. 938–941, 2018.

[17] A. Taha, M. Alrabeiah, and A. Alkhateeb, "Enabling large intelligent surfaces with compressive sensing and deep learning," *IEEE access*, vol. 9, pp. 44 304–44 321, 2021.